NASW-4435

Department of Aerospace Engineering
Auburn University
Auburn, Alabama 36849

Greg Buttram, Keith Horton,
Tim Keeter, Paul Millhouse,
Kelli Newberry, Brian O'Byrne

Senior Design

June 4, 1991

The Langley Turbo-Prop Commuter Design: A Complete Project Description

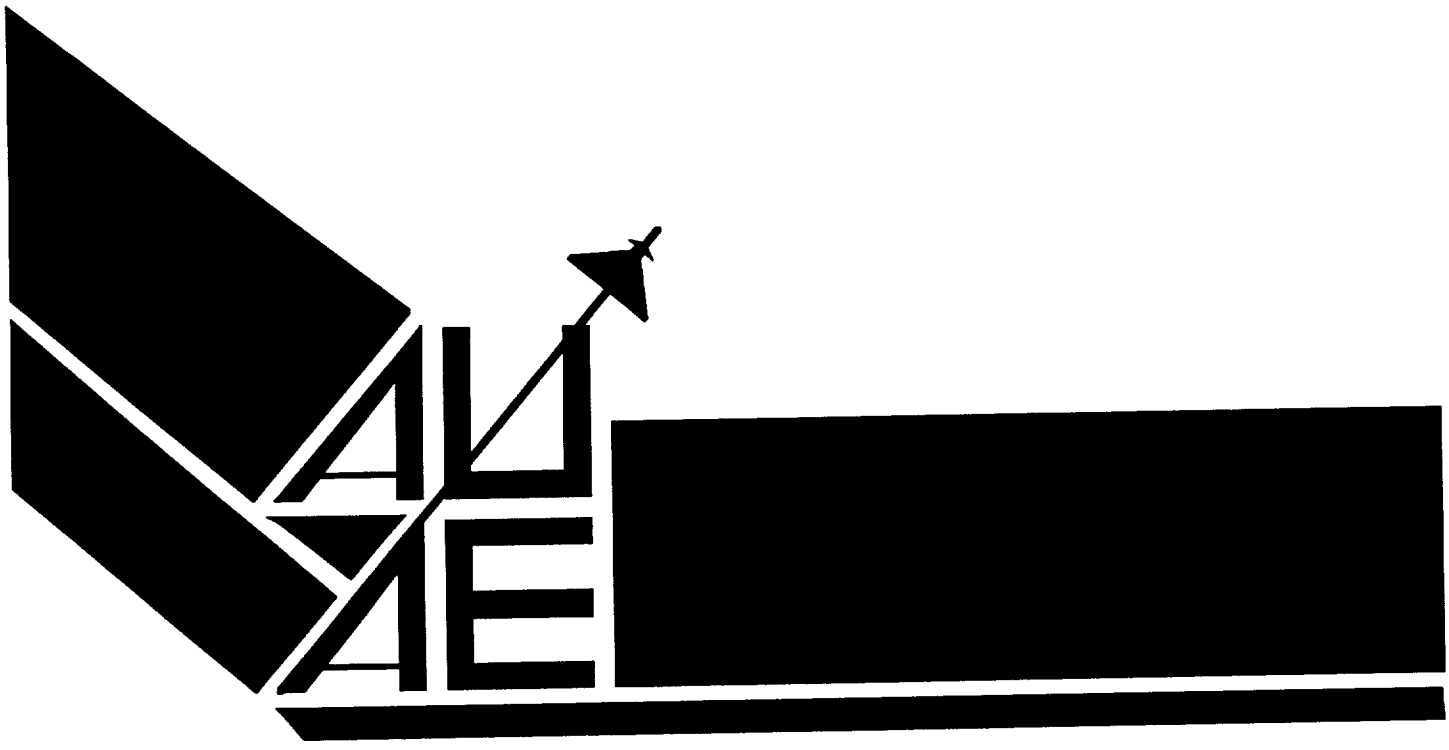

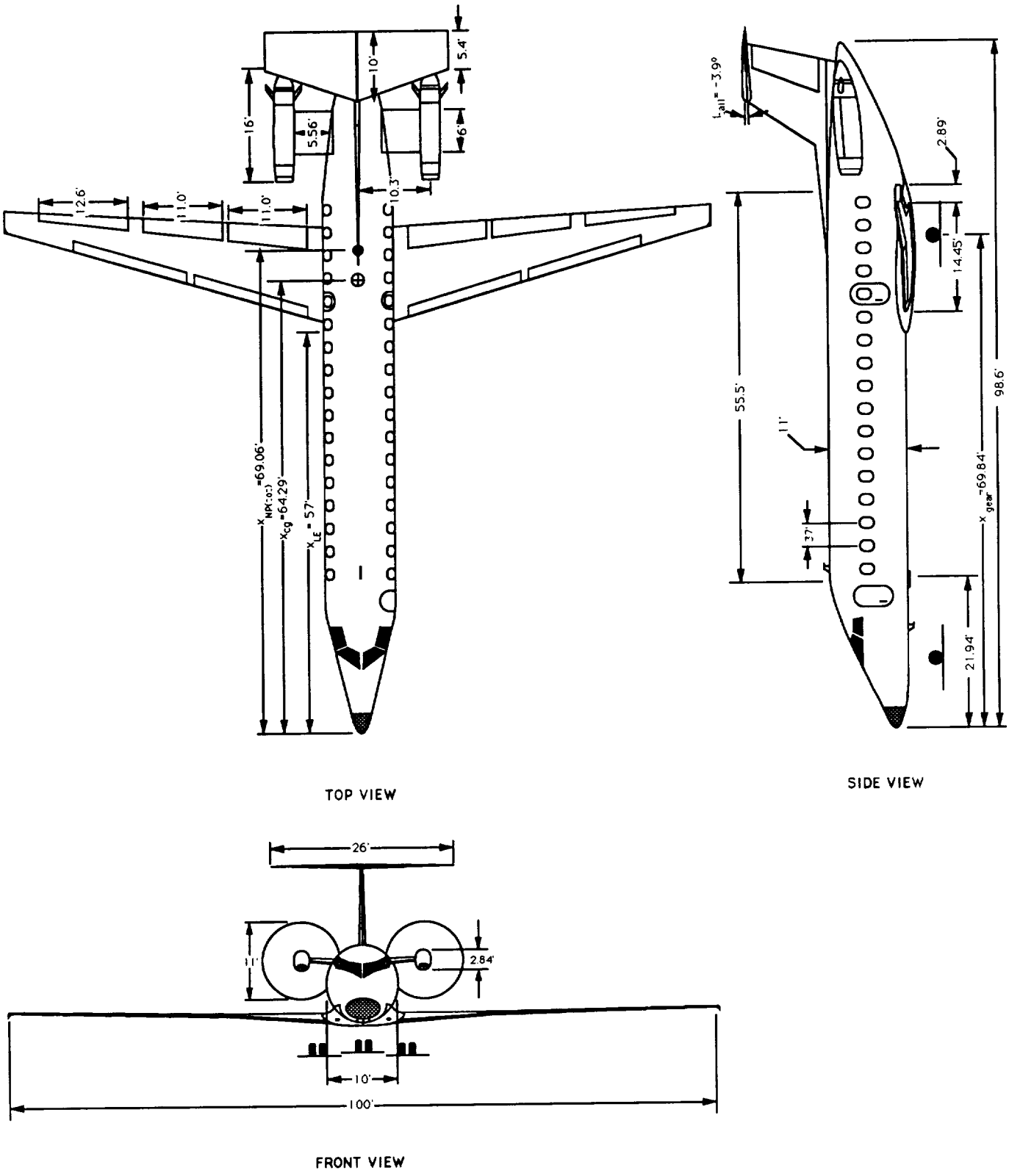

Figure 1. 3-View Drawing

TABLE OF CONTENTS

LIST OF FIGURES

LIST OF TABLES

LIST OF SYMBOLS

Symbol	Description	Units
AR	Aspect ratio	--
b_w	wing span	ft
C_D	Coefficient of drag	--
CG	Center of gravity	ft
C_{HT}	Horizontal tail volume coefficient	--
C_L	Coefficient of lift	--
C_{Lmax}	Maximum coefficient of lift at cruise	--
$C_{Lmax(L)}$	Maximum coefficient of lift at landing	--
C_{LmaxTO}	Maximum coefficient of lift at takeoff	--
$C_{L\alpha t}$	Lift curve slope for the tail	--
$C_{L\alpha WB}$	Lift curve slope for the wing body configuration	--
C_M	Total pitching moment coefficient of aircraft	--
C_{Mo}	Pitching moment coefficient at zero lift	--
C_{MoTOT}	Total pitching moment coefficient at zero lift	--
C_{MoWB}	Pitching moment coefficient at zero lift for wing body configuration	--
$C_{M\alpha}$	Change in pitching moment with respect to angle of attack	--
$C_{M\alpha TOT}$	Total change in pitching moment with respect to angle of attack	--
$C_{M\alpha WB}$	Change in pitching moment with respect to angle of attack for wing body configuration	--
C_{VT}	Vertical tail volume coefficient	--
C_W	Distance to mean aerodynamic chord	ft
i_{TAIL}	Angle of incidence of tail	deg
K	Static margin of the aircraft	--

LIST OF SYMBOLS (continued)

Symbol	Description	Units
L_{HT}	Moment arm for horizontal tail	ft
L_{VT}	Moment arm for vertical tail	ft
Q	Production quantity per year	--
TOP_{23}	Takeoff performance coefficient	--
S_{HT}	Horizontal tail area	ft^2
S_{REF}	Reference area - planform area	ft^2
S_{TO}	Takeoff distance	ft
S_{VT}	Vertical tail area	ft^2
V	Aircraft velocity	knots
V_B	Aircraft velocity at braking	ft/s
V_C	Aircraft velocity at contact	ft/s
V_{50}	Aircraft approach velocity to clear a 50 ft obstacle	ft/s
$\left(\frac{W}{P}\right)_{TO}$	Weight to power ratio at takeoff	lb/hp
$\left(\frac{W}{S}\right)_{TO}$	Wing loading at takeoff	lb/ft^2
W_e	Empty weight	lbs
X_{CG}	Distance from nose of aircraft to center of gravity	ft
X(LE)	Distance from nose of aircraft to leading edge of wing	ft
X_{nTOT}	Distance from nose of aircraft to neutral point	ft
α	Angle of attack	deg
$\Lambda_{C/4}$	Quarter chord sweep angle	deg
Λ_{LE}	Leading edge sweep angle	deg

LIST OF SYMBOLS (continued)

Symbol	Description	Units
Λ_{TE}	Trailing edge sweep angle	deg
σ	Density ratio	--

Abstract

The primary objective of this project was to propose and prove the feasibility of a new, advanced technology commuter aircraft design. This design was to meet certain standards as specified by NASA Langley Research Center. Among these specifications were: short-to-medium range capabilities, low seat-per-mile cost, fuel efficiency, and passenger comfort.

To fulfill these requirements, we have proposed an aircraft which makes use of several progressive technologies, including advanced turboprop engines, natural laminar flow wings, composite materials, and state of the art avionics systems. Our answer to this request for proposal was the product of extensive research of market trends, available technologies, and previous solutions to similar problems.

The conclusions drawn from our research led us to specific solutions to the challenges of this problem. Based on market evaluation, we have found that the optimum size for new regional aircraft is around 50 passengers and have designed our aircraft for this capacity. Recent development in the field of turboprop propulsion has led to powerplants which offer performance comparable to jets. At the same time, these engines offer substantial reductions in operating costs due to lower fuel consumption. We have therefore chosen an advanced turboprop engine. Composite materials, while more expensive to purchase and manufacture, result in decreased costs later through weight savings and ease of replacement. For these reasons, composites will be used extensively throughout this design.

We have outlined and proven the validity of this design concept through careful analysis. We are confident that this design offers a practical and viable solution to the problem considered.

The Langley Turboprop Group:
Greg Buttram
Keith Horton
Tim Keeter
Paul Millhouse
Kelli Newberry
Brian O'Byrne

Introduction

The purpose of this report is to discuss the design of the Langley Turboprop Commuter shown in Fig. 1. The design was undertaken as a response to a request for proposal by the NASA Langley Research Center for the design of a regional transport aircraft to meet the apparent demands of a future market. The provisions as outlined by Langley are listed in Table 1.

Table 1. Commuter Specifications

1. Short-to-medium range capabilities for regional transport
2. Improved passenger comforts and seamless service
3. A speed suitable for a commuter service aircraft
4. Low levels of cabin noise
5. High lift capabilities
6. Materials which meet FAA strength requirements at lower weights
7. Fuel efficiency and low seat-per-mile costs
8. A seating capacity of 35 to 50 passengers

There is no current American design for this type of transportation. Furthermore, the FAA predicts that larger regional aircraft (more than 20 passengers) will dominate the market by the turn of the century.

Originally the design focused on the modification of the Dornier 328. The 328 had many of the same characteristics desired for this aircraft, such as range and mission profile. However, as the design process progressed, it became much different from the 328 with respect to configuration and size. Another aircraft which is similar to the design is the BAe ATP, which has a seating capacity of 64 passengers. The ATP serves as a good base for comparison because it has a similar size and shape, but differs in that it uses wing-mounted tractor turboprop engines, instead of the aft-mounted pusher turboprops found on the proposed commuter. Aft-mounted engines are used to reduce noise levels in the cabin.

Cabin Layout

One of the main objectives in this commuter design is passenger comfort. For this reason, the cabin is designed to maximize passenger accommodations. We studied cabin designs from aircraft similar to ours and modeled the cabin so that passengers will have accommodations similar to first class.

The commuter will have 17 rows of seats with three seats abreast. Seat pitch, or the distance from one seat back to the next, is 37 inches. Each seat will be 25 inches in width, and the aisle will also be 25 inches in width. Each passenger will have five feet four inches of headroom below the storage space allocated for carry-ons. The aisle height will be seven feet one inch. In addition, each passenger will have 4.2 cubic feet of carry-on space located above the seats. These dimensions are illustrated in Figure 2.

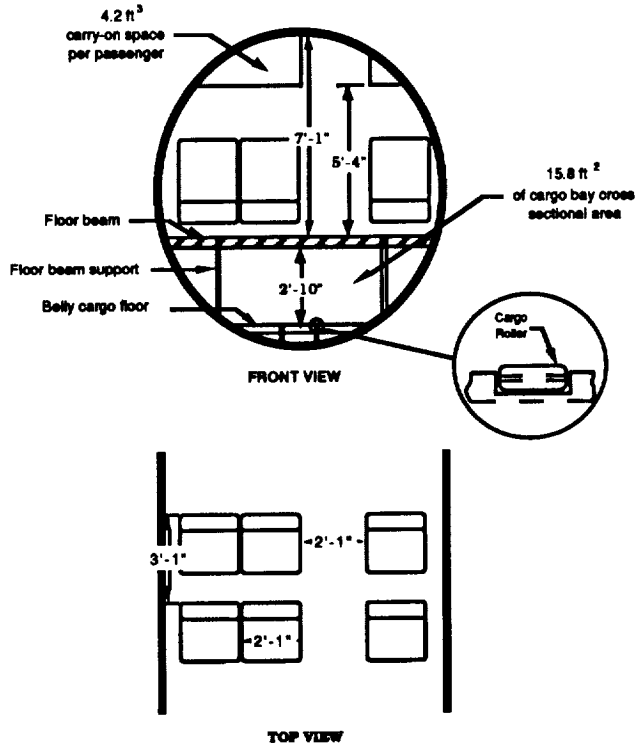

Fig. 2 Cabin and Cargo Layout

Aerodynamics

To begin the analysis of the aerodynamics of the proposed aircraft, we derived areas for the wing, horizontal tail and vertical tail surfaces. From these derived areas, the appropriate shapes of the surfaces were determined to meet structural constraints as well as to maximize the possible aerodynamic gains.

First, an equation was found in *Airplane Design : Part 1 : Preliminary Sizing of Airplanes* that with a few simple inputs yields a wing area which will be used in the remainder of the aerodynamic and stability calculations.[1]

The equation used is

$$\frac{\left(\frac{W}{S}\right)_{TO}\left(\frac{W}{P}\right)_{TO}}{\sigma\ C_{L_{MAX_p}}} = TOP_{23} \quad , \qquad (1)$$

where $(W/S)_{TO}$ is the take-off wing loading and $(W/P)_{TO}$ is the take-off weight divided by the total engine power in shaft horse power (shp). σ is the ratio of the density at altitude to sea level atmospheric density. The maximum C_L used in this equation is the largest lift coefficient of the airfoil in the take-off configuration, divided by 1.21 for FAR Part 23 regulations. The TOP_{23} term of the equation is determined by using another equation which incorporates desired take-off distance. This relation, established through extensive analysis of all forms of general aviation, is

$$\text{Take-off Dist.} = S_{TO} = 8.134TOP_{23} + (0.0149TOP_{23})^2. \qquad (2)$$

Some typical lift coefficients for the cruise, takeoff and landing configurations will be useful for later calculations. For a regional turboprop aircraft:

$$C_{Lmax} = 1.5 \text{ to } 1.9$$
$$C_{Lmax(TO)} = 1.7 \text{ to } 2.1$$
$$C_{Lmax(L)} = 1.9 \text{ to } 3.3. \quad (3)$$

In finding the desired wing area, an estimated total weight of 40,000 lbs and a single engine output of 6400 shaft horsepower was used. We considered the "hot day in Denver" case for the density of the air at take-off and chose an atmospheric density corresponding to a 12,000 foot altitude on a standard day. Through an average of statistical data on regional turboprop aircraft, a take-off C_L of 1.9 was chosen. Finally, after studying the goals and intentions of this aircraft, we determined 3200 feet to be a desirable take-off roll. Through the use of these two equations, the S_{ref} area was calculated to be 867 square feet.

After the wing area was determined, the next task was to develop a wing shape that would best meet the needs of the aircraft. High aspect ratio wings are beneficial in that they have low induced drag characteristics, good for single engine climb-outs and gliding flight. However, a structural penalty must be paid for high aspect ratio wings since they are usually very long and slender. An aspect ratio of 11.53 was chosen to allow drag benefits without structural complexity. The leading edge of the wing is swept to assist in achieving cruise Mach numbers greater than 0.6, resulting in a smaller taper ratio. The final configuration for the wing is illustrated in Figure 3.

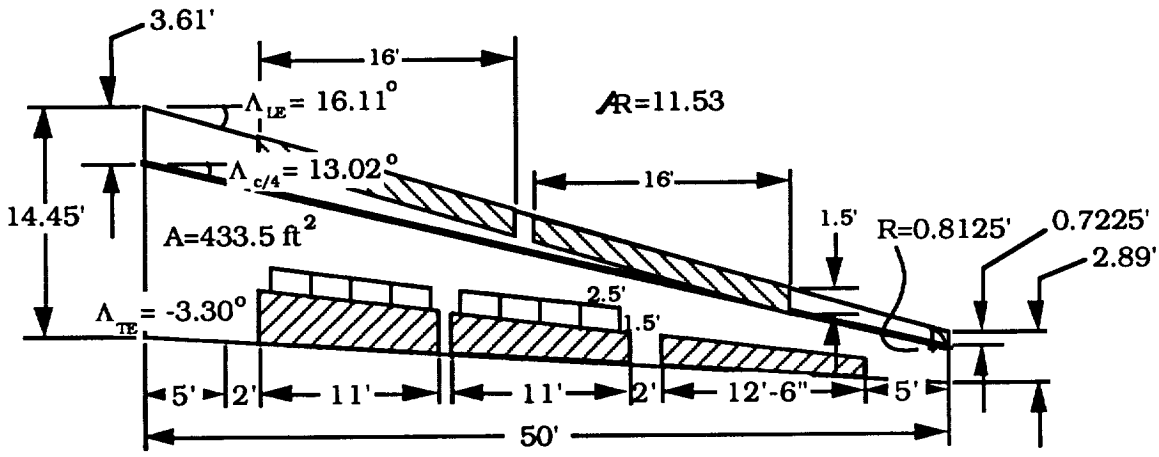

Wing

Fig. 3 Schematic of Wing

The natural laminar flow airfoil, model NLF(1)-0215F, was chosen for its excellent performance characteristics at the desired cruise speed of 360 knots (Fig. 4). Laminar flow airfoils delay the transition to turbulent flow over the wing, thus preventing the high parasite drag of turbulent flow. A good laminar flow airfoil like this one combined with smooth fabrication methods can produce a wing with laminar flow over about 50-70% of the wing.

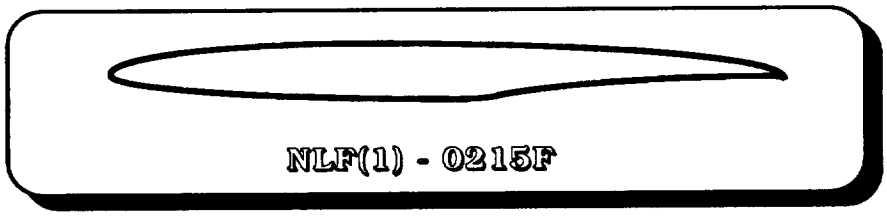

Fig. 4 The Natural Laminar Flow Airfoil Model

Since this chosen airfoil stalls at a C_l of approximately 1.5, high lift devices are necessary to achieve greater take-off and landing performance. Our approximated maximum take-off C_L has been previously stated as 1.9.

The set specification was met through the use of double slotted Fowler flaps and leading edge slats. Likewise, in the landing configuration, a C_L of 2.5 was needed, thus requiring the full use of our proposed high lift devices. The Fowler flap increases the effective camber and wing area, creating greater lift capability at low airspeeds. The slats, aside from extending the stall angle of the wing, also create a larger wing area and camber.

At this point, the control surface design and size need to be calculated. From Raymer's design book, the ailerons, flaps, and slat sizes can be determined[2]. The ailerons typically extend from about 50%-90% of the wing span. With this long wing, a 40% flap is appropriately sized at about 20 feet long. The aileron is about 30% wing span which equals 12.5 feet in length. This should provide sufficient roll control for the aircraft.

The flaps occupy the part of the wing inboard of the wing aileron. If a large maximum coefficient of lift is required, the flap should be as large as possible. In order to meet the requirement for a short take off and landing aircraft, large flaps are needed to produce the desired results. As stated above, double slotted Fowler flaps will be used. Along with increasing the camber to provide lift, the deployed Fowler flap will also increase the wing area. Each flap is 11 feet long and is spaced 1.5 feet apart (see Fig. 2). The flaps and ailerons extend from the trailing edge of the wing to the three quarter chord line and are in a constant taper ratio with the three quarter chord line of the wing. According to Raymer, this configuration will help prevent flutter tendencies on the wing itself.

Slats work well to complement the slotted trailing edge flaps. They increase camber and wing area to increase lift on the wing. From looking at many similar general aviation designs, the slat was chosen to extend 70% of the wing span. When the slat is deployed, the increase in camber must be experienced by a large portion of the wing, therefore 70% is a realistic number. There are two slats on each side of the airplane, each being 16 feet

in length and 1 foot apart.

The mean aerodynamic chord length and center of gravity location were calculated for the wing. The CG location was found to be 10.6 feet from the leading edge of the wing along the center line and the mean aerodynamic chord is 9.948 feet long.

With the wing information and Raymer's book, the horizontal and vertical tail areas can be determined by using the Tail Volume Coefficient Method. The formulas

$$S_{vt}=C_{vt}b_wS_w/L_{vt}$$

and

$$S_{ht}=C_{ht}C_wS_w/L_{ht} \qquad (4)$$

are the equations for the tail areas. L_{vt} and L_{ht} are the moment arms for the tail. For an aircraft with aft mounted engines the moment arms are 25-30% of the length of the fuselage. The fuselage length is 98.6 feet, so L_{vt}=27.4 feet and L_{ht}=28.4 feet. S_w is the reference area for the wing and S_w=867 square feet, b_w is the wing span which is equal to 100 feet and C_w is the mean aerodynamic chord for the wing, which is 9.948 feet long. The tail coefficients C_{vt} and C_{ht} can be estimated from Table 6.4 in Raymer's design book. They were found to be C_{vt}=.0395 and C_{ht}=.6585. From this information S_{vt} was calculated to be 125 square feet and S_{ht} equals 200 square feet.

After the tail areas have been found the tail geometry and the rudder and elevator size can be determined. In Table 4.3 of Raymer's book, the aspect and taper ratio of a T-tail aircraft can be estimated. The leading edge of the horizontal tail is normally set about 5 degrees more than the sweep of the wing. This tends to make the tail stall after the wing which is

an important control feature. The leading edge of the horizontal tail is 19.5 degrees. The vertical tail sweep usually varies between 35-55 degrees for most airplanes. The vertical tail has a sweep of 35 degrees since the airplane will have a maximum speed of less than Mach 1. With this information, the tail geometry for both the horizontal and vertical tail was completed (See Figure 5). The mean aerodynamic chord and the CG location for both the horizontal and vertical tails were calculated. For the horizontal tail the mean aerodynamic chord is 7.93 feet and the CG location is 6.03 feet from the leading edge of the tail measured down the centerline. The mean aerodynamic chord for the vertical tail is 10.34 feet and the CG is located on the mean aerodynamic chord line 8.0 feet from the leading edge of the root chord.

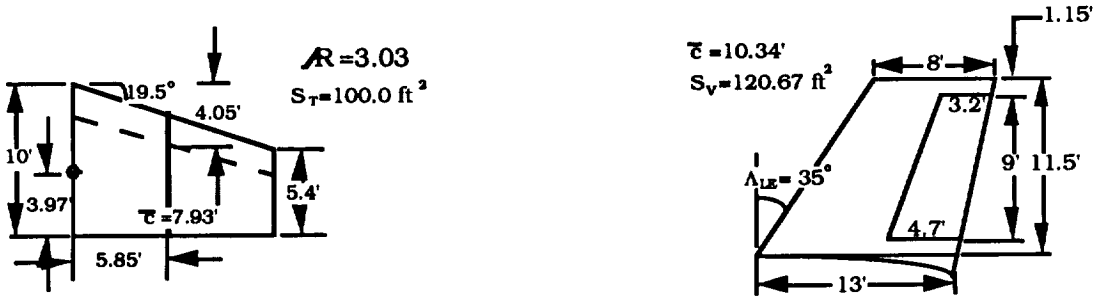

Horizontal Tail **Vertical Tail**

Fig. 5 Horizontal and Vertical Tail Configurations

The primary control surfaces on the tail are the stabilator and the rudder. Rudders usually begin at the side of the fuselage and extend to about 90% of the tail span. This control surface is usually 25-50% of the tail surface chord and has 25-30% of the aerodynamic balance. The rudder was chosen to be about 78% of the vertical tail span or 9.0 feet and 40% of the chord. The stabilator is an all moveable horizontal tail which regulates pitch by changing the incidence of the horizontal surface. [2]

Stability

The stability of an aircraft is essential to its operation in flight. The extent of the stability analysis on the plane was limited to the static longitudinal stability combined with some general theory considerations for the static lateral stability problem.

The static longitudinal stability analysis requires a number of variables to be taken into account. First, the locations of all "fixed" elements of the aircraft and their respective weights were calculated. All distances in these calculations are measured from the tip of the nose cone of the aircraft. The various component weights were derived through the use of average structural weights per unit area, which were multiplied with the previously calculated surface areas. Table 2. shows the values used in this center of gravity (c.g.) calculation.

Table 2. Component Weights, CG Positions, and Moments of the Aircraft

Component	Weight (lbs)	Position (ft)	Moments (ft*lbs)
Nose Gear	217	11.25	2441
Fuselage	9731	57.19	556,496
Two Engines	2678	87.35	233,923
Vertical Tail	1054	90.60	95,492
Horizontal Tail	1679	97.43	163,585
"Dry" Wing	4050	67.6	273,780
Main Gear	1225	69.84	85,554
Empty Weight	**20,634**		
51 Passengers (180 lbs. ea.)	9180	49.69	456,154
Fuel (max. loading)	8800	67.6	594,880
Front Baggage	1300	49.2	63,960
Aft Baggage	1300	79.5	103,350
Misc. Weight	**20,580**		
GTOW	**41,214**		

In considering the complicated series of calculations involved with determining the wing location, we used a spread sheet program capable of allowing the variation of the position of the wing/gear/baggage as well as the incidence angle of the horizontal tail. These two factors dictate the final lift, pitching moment and static margin characteristics important to the stability of the airplane.

It can be seen that the position of the wing will determine where the neutral point of the aircraft will lie. At the same time the position of the wing changes the location of the aircraft's c.g. As both of these positions vary, the lift required of the tail changes which in turn dictates the incidence of the tail. Underlying through all of these values is the resulting zero-lift pitching moment (C_{Mo}), the slope of the pitching moment curve ($C_{M\alpha}$) and the final total aircraft pitching moment (C_M). These three values combined with the static margin of the aircraft (K) ultimately prove the aircraft to be either : a) stable and trimmable, b) stable and untrimmable, c) unstable and trimmable, or d) unstable and untrimmable.

The stability characteristics of this airplane at various loading conditions are shown in Table 3.

Table 3. Stability Characteristics at Various Loading Configurations

Loading Condition	C.G. Location	Static Margin	Cmα
*Fully Loaded (51 Pass & Bags, Full Fuel)	64.29	0.479	-0.0533
* No Pass & Bags, Full Fuel	68.16	0.0905	-0.0156
* No Pass & Bags, Half Fuel	68.24	0.0827	-0.0148
* No Pass & Bags, 20% Fuel	68.29	0.0769	-0.0143
* Empty (No Pass & Bags, No Fuel)	68.34	0.0724	-0.0138

No calculations were performed to determine lateral stability; however, we did apply theory to our general design to promote lateral stability. First, the wings were given approximately 5 degrees of dihedral in order to establish roll stability. Many low wing aircraft use this dihedral because it causes the plane to tend to return to straight and level flight when placed in some bank angle. This tendency occurs because the aircraft slips downward while in the turn, thus increasing the effective angle of attack on the lowered wing. This increased effective angle of attack increases the lowered wing's lift and causes the plane to return to equilibrium. This concept of roll stability applies in level flight because if a gust suddenly lifts a wing, the plane will inherently return to level flight, thus preventing any control input to make correction. [3]

The vertical tail and rudder were chosen to have large enough surface areas to produce any needed yawing moments necessary for side-slip or unbalanced engine thrust. The dorsal fin leading into the vertical tail separates the incoming flow to the tail lowering the pressure drag on the tail. It also serves the more important role of stabilizing the aircraft in a spin condition. This added tail area helps to stabilize the violent yawing experienced during a spin. In all, the lateral stability elements have been estimated to yield the desired stability characteristics.

Performance

An analysis of aircraft performance is a critical aspect of the design process. To predict the performance parameters of the aircraft, we had to first estimate the drag polar using Jan Roskam's *Methods of Estimating Drag Polars of Subsonic Aircraft.* [4] Calculations yielded the following relation:

$$C_D = 0.0183 + 0.032\ C_L^2. \qquad (5)$$

The propeller efficiency was calculated using Hamilton Standard publication PDP 6101 revision A, "Generalized Method of Propeller Performance Estimation." [5] After a series of calculations, the propeller efficiency was calculated to be 0.76 at cruise altitude.

The next consideration was takeoff performance. Using a C_{lmax} for the airfoil section, a C_{Lmax} at takeoff was calculated to be 1.49. This value yielded a stall speed of 96.4 knots at a density altitude of 12,000 feet. The takeoff velocity was calculated to be 99.3 knots with a total takeoff distance, as per FAR part 25, of 3526.3 feet. The maximum rate of climb from this density altitude at takeoff speed was determined to be 1762.5 feet per minute, and climb velocity was calculated, per Federal Aviation Regulations (FAR) part 25, to equal 107.9 knots. [6]

Several quantities were necessary for calculating cruise performance. The lift coefficient of the fully loaded aircraft, cruising at a velocity of 360 knots and an altitude of 25,000 feet, was determined to be 0.323. The lift coefficient for maximum range, defined by a cruise value of C_L/C_D of 11.5, was determined to be 0.412 with a corresponding drag coefficient of 0.0237. The lift coefficient for maximum endurance and minimum power required, defined by the maximum value of $C_L^{1.5}/C_D$, was calculated to be 0.7414, with a corresponding drag coefficient of 0.0359. These values were then used to calculate a maximum range of 2046 nautical miles. Also, the specific range was computed to be 0.233 nautical miles per pound of fuel. [3] Figure 6 shows the flight envelope for cruise conditions (flaps and gear fully retracted).

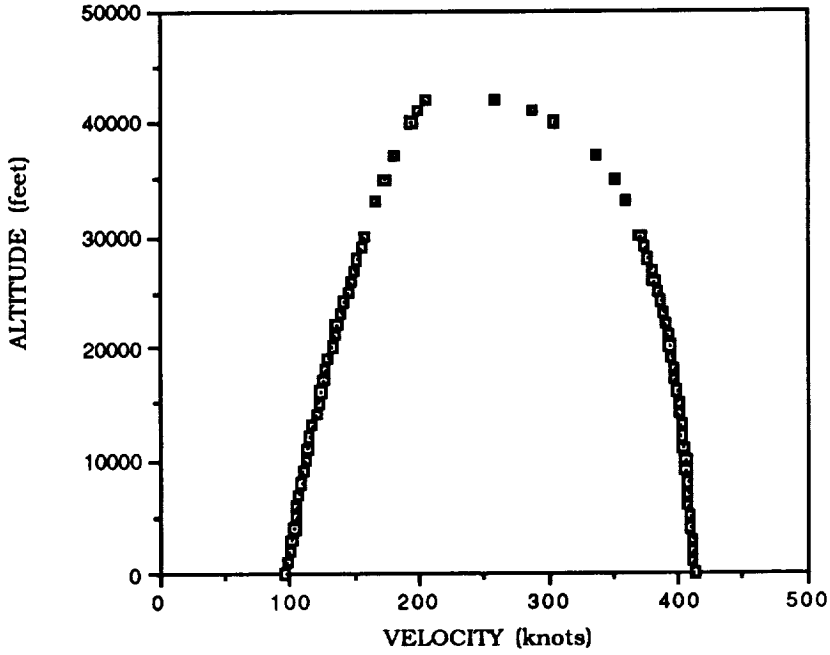

Fig. 6 Flight Envelope

Certain relevant aspects of turning flight performance were also considered. The load factor plotted versus equivalent airspeed for turning flight is shown in Figure 7. This graph illustrates a maximum load factor of 2.85. Next, the load factor for a standard two minute turn was found to be 1.126, with a turning radius of 6176 feet and a bank angle of 27.36 degrees.

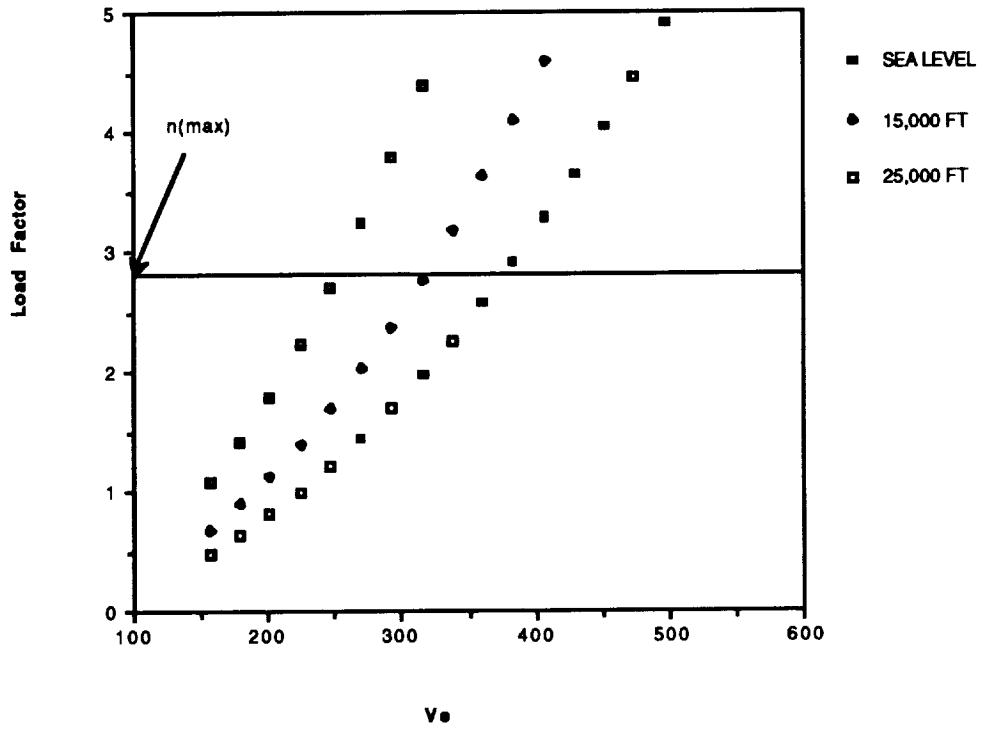

Fig. 7 Load Factor versus Equivalent Airspeed for Turning Flight

Landing performance was also evaluated according to FAR part 25 guidelines. The velocity required to clear a 50 foot obstacle was determined to equal 107.7 knots and the aircraft's velocity when it makes contact with the ground is 95.3 knots. The velocity of the aircraft at braking was determined to be 81.0 knots. These velocity values were then used to determine the various forces and distances associated with landing. The total landing distance, as per FAR part 25, was calculated to be 3711.3 feet.[6]

Propulsion

In order to meet the goals for this design, the propulsion system must meet, and in some cases exceed, current standards in propulsion technology. These standards include such subjects as fuel efficiency, cruise

speed, and interior and exterior noise levels. The propulsion system chosen for this design is an advanced turboprop engine in a pusher configuration. The advanced turboprop design offers a high propulsive efficiency, at a relatively high Mach number, as compared to both the turbofan and the conventional turboprop in Figure 8. These engines will be mounted on either side of the far aft portion of the fuselage below the high T-tail. As described below, these choices are best suited to allow this design to meet these standards. By choosing the advanced turboprop engine, the commuter aircraft could reach a cruise Mach number of 0.6. Aft mounted engines will reduce interior noise levels and allow clean flow over the wing.

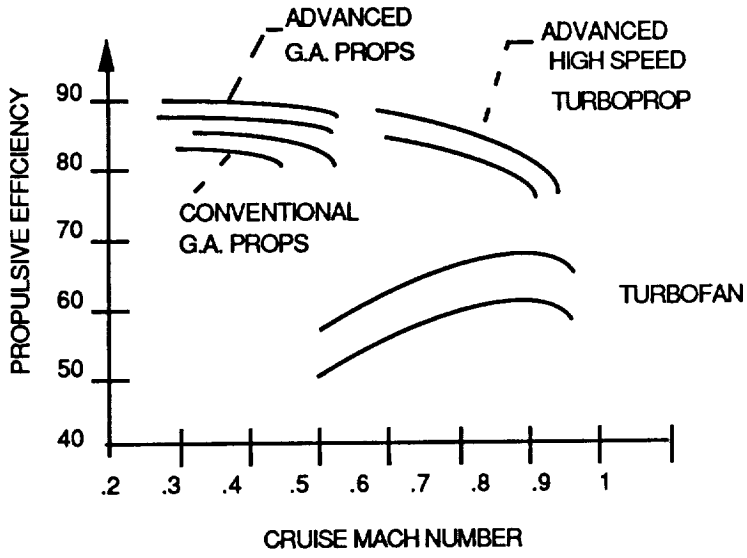

Figure 8. Propulsive Efficiency Trends

Allison Gas Turbines is a major test and manufacturing company of some of the worlds more advanced turboprop engines. Currently, Allison is in the late stages of design for a prototype turboprop engine, the GMA 2100, which has demonstrated 6,400 shaft horsepower in a series of successful ground tests. The core of this engine, the T406, is a front drive

free turbine turboshaft gas turbine engine, and currently powers the V-22 tilt rotor aircraft.

The ground tests have generated data that will be used to analyze the stresses on the prototype engine's propeller. The 11 foot diameter propeller is a Dowty Rotol propeller. Analyses conducted by Allison indicate that the blade stresses are well below the limit of the propeller blades.

The Dowty Rotol blades are made of a polyurethane foam core sandwiched between two carbon fiber spars that run from the blade tip to the root. This assembly is then covered with a glass fiber or a carbon/fiber/glass-fiber shell, and spray coated with a protective polyurethane. According to Max Kelley, sales and marketing director for Dowty Rotol, this process produces very low weight blades which enables the control system to be relatively simple. [7]

The fuel system of the prototype is the most unusual feature of the engine. Control of both the propeller and the fuel system is integrated into a single full authority digital engine control, known as FADEC. Therefore, the GMA 2100 has only one throttle to control engine power, propeller blade pitch, and propeller synchronizing and synchrophasing functions (Fig. 9).

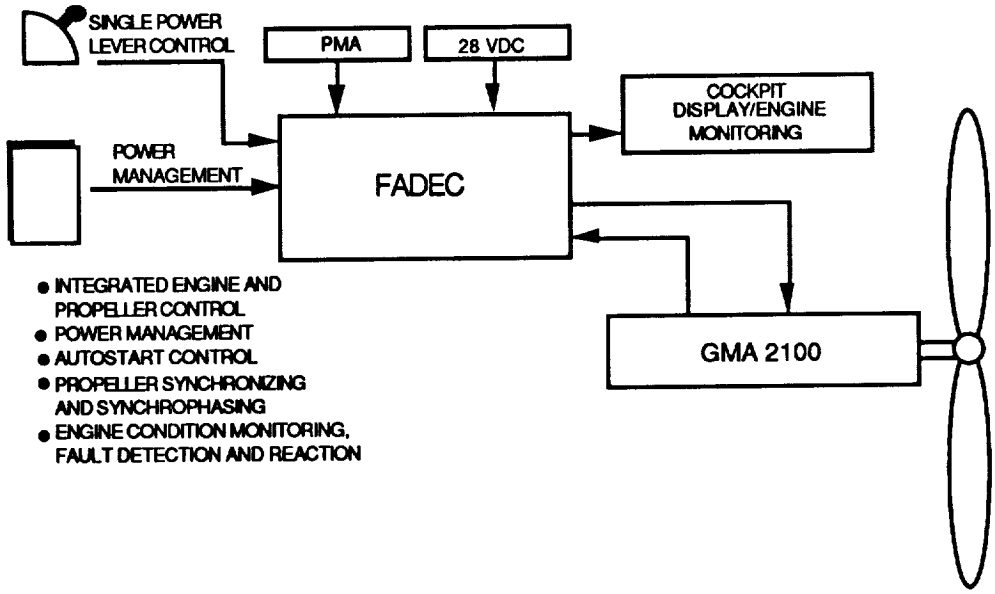

Fig. 9 Schematic of FADEC

The T406 core engine is composed of a 90% efficient compressor, an annular combustor, and a two stage air cooled turbine with single crystal material. The high pressure compressor is composed of variable geometry vanes to enhance the speed performance of each part. This type of design makes use of steel blades and vanes to make the compressor less susceptible to corrosion and catastrophic failure, while providing a balance between durability and light weight. The fuel pump, hydraulic pump, starter and electric power for FADEC are powered by the high speed rotor driven accessory gearbox. The gearbox contains an engine driven permanent magnet alternator (PMA), backed up by a 28-volt DC power source.

The GMA 2100 has been designed for quick and easy maintenance with standard hand tools. Other features include no rigging or calibration, easy engine removal and installation, engine monitoring system fault isolation, and a line replaceable gearbox. [8]

As a result of the highly efficient turbomachinery components being developed in the T406 program, the GMA 2100's fuel burn or esfc is only

about .35-.36 lb/lb$_f$hr. Figure 10 compares the 40% improved fuel consumption of the GMA 2100 engine with older technology turboprop engines

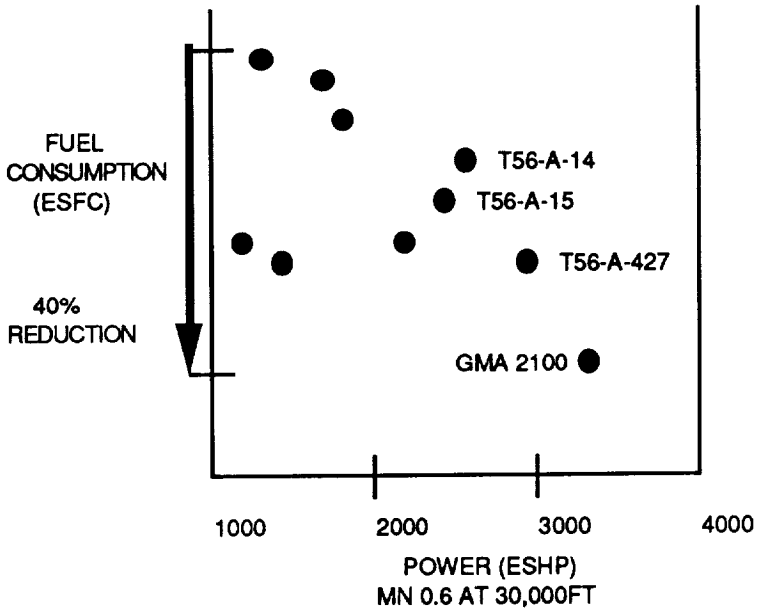

Fig. 10 Comparison of Older Technology Turboprops and the GMA 2100 in Fuel Consumption [8]

Structures

The structural layout of the wing is one of the most crucial design considerations. A wing structure must be able to easily withstand loads from lift, drag, and thrust components of the aircraft, while also serving dual purposes such as a fuel and landing gear storage.

The wing design for this commuter was based on *Airframe Structural Design* by M. C. Y. Niu.[9] The wing will use spars made of high strength composites because the wing is long, thin and wet. A conventional front-rear spar arrangement was selected because a single main beam is only

desirable in the case of a highly swept wing. Using this front-rear configuration allows the central part of the wing to transfer all loads to the fuselage. The front spar is located at 15% chord and the rear is located at 60% chord. At least 5% chord is left between the rear spar and the nested flaps to allow for control system elements. For strength and weight efficiency, the beam section should have the largest possible radius of gyration. We will use a shear-web style beam instead of a truss-web configuration because a truss-web beam has little to no redundancy, seriously affecting its fail-safe characteristics. Webs will carry loads even when they are severely damaged. Cost will also be lower for a web design because they require only a simple cutting operation.

The ailerons are laid out with the leading edge parallel to the rear spar. Ailerons should not exceed 30% of the wing chord in order to leave room for the rear spar cap width, the aileron gap, and control systems. Flaps can run the entire distance of the wing inboard of the ailerons, with the same chord length ratio as the aileron.

There are two basic styles of rib arrangement: spanwise and parallel to the flight path. This design will utilize a spanwise arrangement, which is conventional, because it has several structural advantages over a flight path layout. First of all, a spanwise arrangement is lighter than a parallel arrangement because the rib lengths decrease in the outboard direction, whereas parallel ribs require a greater amount of material. Since 90 degree angles are easier to work with mechanically, the manufacturing cost is lower for spanwise ribs. Furthermore, spanwise rib arrangements require less riveting, so the aerodynamic contour of the wing will not be disturbed as much. Initially, ribs are located at each aileron and flap hinge. Then they are placed according to wing panel area, with reinforcement ribs for supporting landing gear and fuel tanks.

Spanwise stringers need to run parallel to each other at constant chord percentages. Some stringers are discontinued at intervals if they are not needed at the tip. Skin-stringer panels must allow for an optimum ratio of stiffener area to skin area of approximately 1.5, assuming an equal bending stress in the skin and stiffener. A widely used stiffener shape that provides an area ratio of 1.5 is the z-shape stiffener.

We will use integrally stiffened panels with the z-shape instead of separate skin and stringer panels because they have been proven effective as light-weight, high-strength constructions. They reduce the amount of sealing material required for pressurized fuel tank structures, and increase joint efficiencies under tensile loading. Integrally stiffened panels also allow for higher stiffener compression loads because they do not have attachment flanges. A smoother surface from reduced attachments increases the nonbuckling characteristics of the skin and improves flight performance. The structure is also much lighter, providing weight reductions of up to 10 to 15 percent. Figure 11 is a complete illustration of the structured wing .

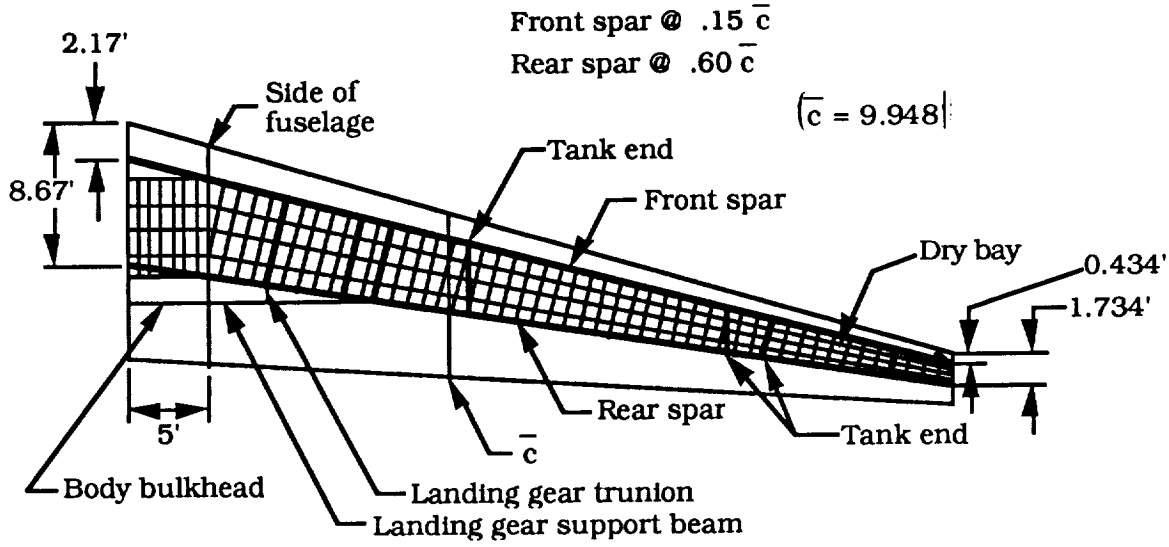

Fig. 11 Structural Wing Schematic

The fuel tanks will be a leak-proof integral design. The spanwise arrangement is dictated by balancing the aerodynamic center for various fuel loads. Since fuel weight acts in the direction opposite to wing bending, thus providing relief to wing moments, the fuel will be used from the inboard outward. As the fuel is used, the airload on the wing will be reduced because of the lowered gross weight. For these reasons as well as safety considerations, center tanks within the fuselage should be avoided, unless they are essential for long range flight.

The point where the wings join the fuselage is a critical area as far as structures are concerned. Since the wings produce large bending moments, the structure must be designed so that these moments will pass between the wings through the fuselage. There are five basic types of wing carrythrough box structures: the space truss, the conical box, the minimum rib and splice design, the built-up variable box, and the constant depth box. The space truss is highly redundant, making it very heavy as well as inefficient for concentrated loadings such as landing gear supports. The conical box is also a poor choice because it is inefficient for bending and fuel containment, and has the highest manufacturing cost. The built-up variable box has good fuel capacity, relatively good damage tolerance, but is not practical for passenger aircraft. The minimum rib and splice design has several advantages such as high efficiency and low manufacturing costs. However, this design has poor damage containment capabilities due to the low number of ribs and splices. A constant depth box (Fig. 12) is desirable because of its simple geometry and the resulting low manufacturing cost. In addition, it provides a total continuity in the upper cover, and minimizes spar and rib sizes, thus lowering the weight.

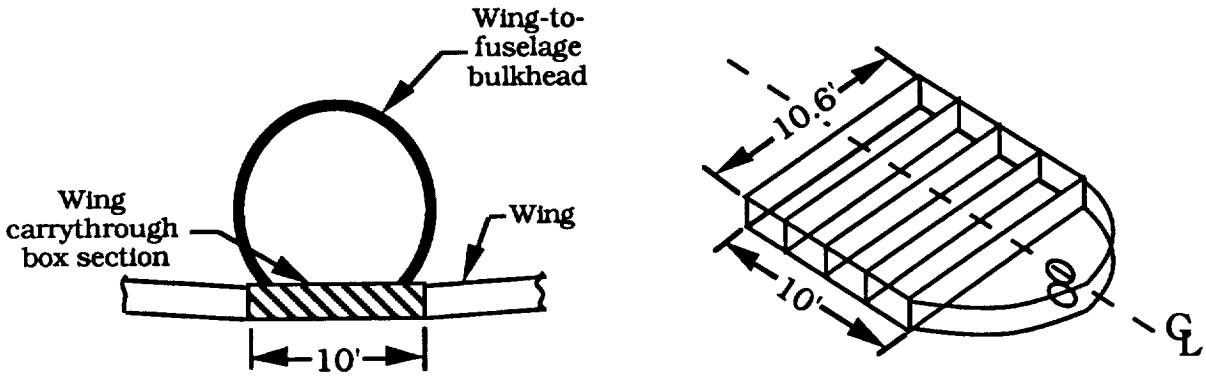

Fig. 12 Cross Section and Isometric of the Wing Carrythrough Box

The fuselage of the aircraft is a semi-monocoque construction, or simply a stiffened shell. There are three means of supporting loads--longitudinal elements, transverse elements, and the external skin. Longerons and stringers are the longitudinal elements; longerons carry the largest portion of the bending moment. Similarly, stringers carry axial loads induced by the bending moment, as well as stabilizing the external skin. As in the wing skin, the fuselage skin serves to carry shear loads. These shear loads arise from applied external transverse forces, torsional forces, and cabin pressure.

Transverse elements consist of frames and bulkhead. Since the frames carry a relatively small load, they generally serve to maintain the shape of the fuselage and prevent structural instability by reducing stringer length. Bulkheads, however, occur at critical loading points, such as at cutouts in the fuselage (windows, doors, and access panels). In addition, bulkheads will be concentrated at the wing carrythrough box and at the rear engine mounts. Pressure bulkheads will be located at the front and rear of the fuselage. [9]

Another important consideration in the fuselage design is the allocation of sufficient space for cargo below the main cabin area. Assuming

that each passenger will need nine cubic feet of storage, we determined that our aircraft needs a maximum of 459 cubic feet for cargo. The cargo area will have a cross-sectional area of 15.8 square feet (Fig. 2); therefore, 34.8 feet of the total cabin length must be reserved for cargo storage. This should not present a problem because the wing carrythrough box and landing gear should only account for a maximum of 14.45 feet of the 55.5 foot cabin length.

The pylons for mounting the engines are a critical structural feature. At the pylon-fuselage juncture, three reinforced fuselage bulkheads will be used to support the sizable loads generated by the weight and thrust of each engine. The pylon itself will be modeled as a hollow structure supported by rods. The cross section of the pylon will be a geometrically aerodynamic shape to reduce drag (see Fig. 13).

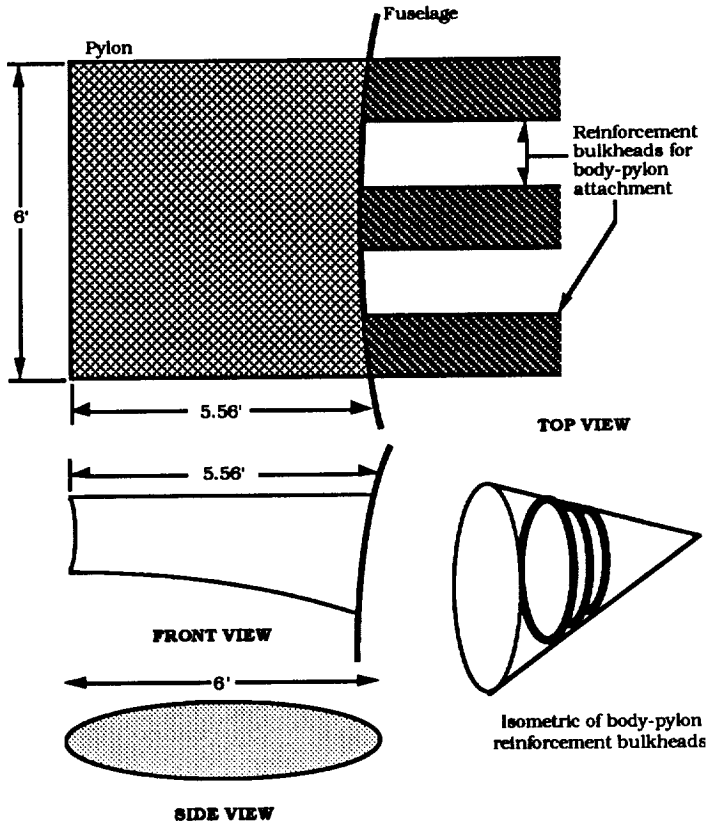

Fig. 13 3-View and Isometric of Engine Mount Pylon

The final structural area considered is the landing gear. A tricycle arrangement with two wheels on the nose gear, and two wheels on each main gear will be used. The main gears will be stored in a joint wing/fuselage junction (Fig. 14). The nose gear is designed to support 15% of the gross takeoff weight, and the main gears will split the remaining 85%. Wheel widths, as a functions of the weight acting upon each gear, were determined to be 8.19 inches for the main gears and 3.9 inches for the nose gear. The wheel diameters, which are also functions of the gear loading, were computed to be 28.6 inches for the main gear, and 17.8 inches for the nose gear. [2]

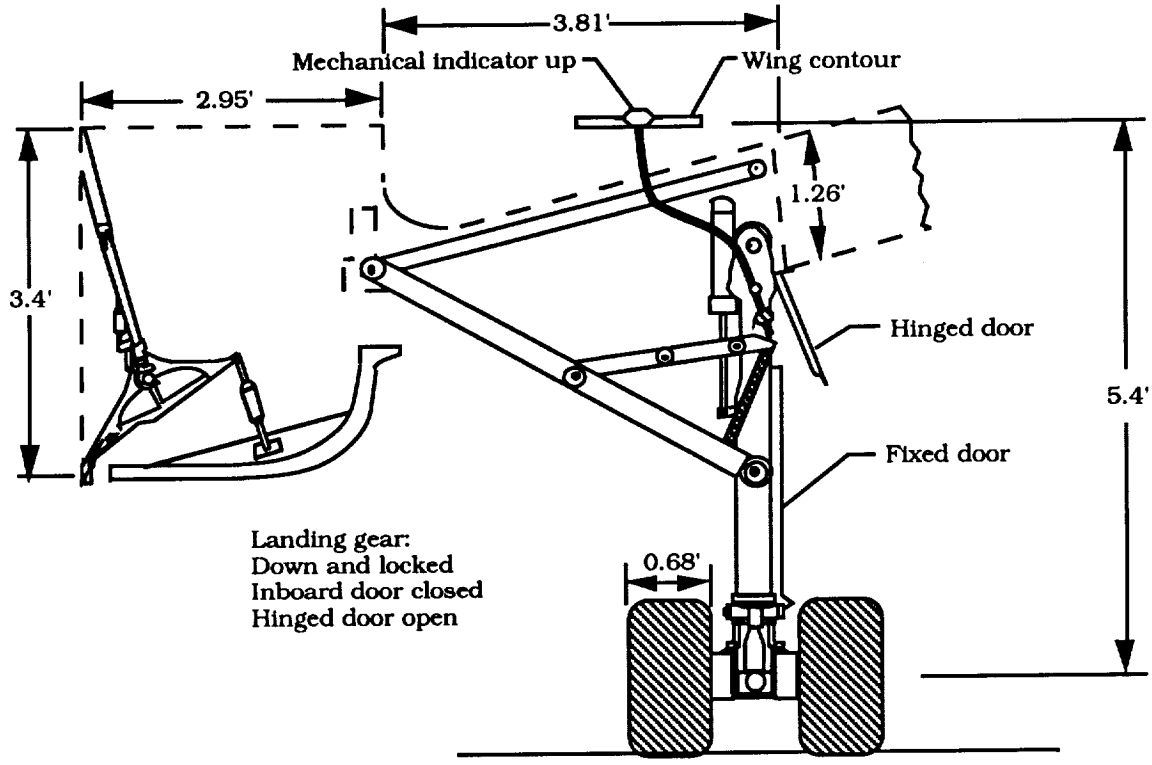

Fig. 14 Schematic of Landing Gear

Materials

Materials selection involves various considerations, and is often a compromise between mechanical properties and cost and manufacturing. Historically, the most important decisions are based on mechanical properties, such as strength, toughness, and corrosion resistance. Other important decisions are based upon producibility, cost, and fabrication characteristics. [9] Aside from cost penalties, a reduction in empty weight is an excellent means of reducing lift induced drag, and therefore expended fuel. Studies have shown that a weight reduction of only one kilogram is worth at least $35 per year in fuel savings. [10]

Since weight is an important consideration, we plan to use as many composite and advanced metal alloys as possible. Among the advanced materials considered are carbon-fiber composites and aluminum lithium (Al-Li).

Carbon-fiber composites, such as graphite-epoxy, are the most commonly used composites because they are easily molded and have excellent strength-to-weight ratios. [2] Graphite with an epoxy matrix has a theoretical tensile strength of about 200,000 pounds per square inch and weighs only about 0.055 pounds per cubic inch. This weight is one half that of aluminum and one sixth the weight of steel. [11] In other words, members made from graphite epoxies might be the same size as aluminum members but weigh only one half as much.

Carbon-fiber composites are suitable for the areas critical to the structural integrity, such as the wing carrythrough box, fuselage bulkheads, and pressure bulkheads. Also, since graphite epoxy has high corrosion-resistance and durability, it may replace members which were previously made of conventional materials, such as fairings, doors, and some leading edges. [12] Other applications for fiber composites would include glass fiber

coatings on the nose cone and the fuselage rear cone.

Aluminum lithium is less dense than conventional alloys with comparable strengths, and it also has a higher stiffness, leading to further weight savings. [10] Specifically, aluminum-lithium is 10% lighter and 10% stronger than other alloys, and has a much greater fatigue performance. Al-Li will be used on some leading edges, fuselage skin, skin for doors and access panels, and fuselage stringers. [13] Figure 15 gives a full illustration for the aircraft material distribution.

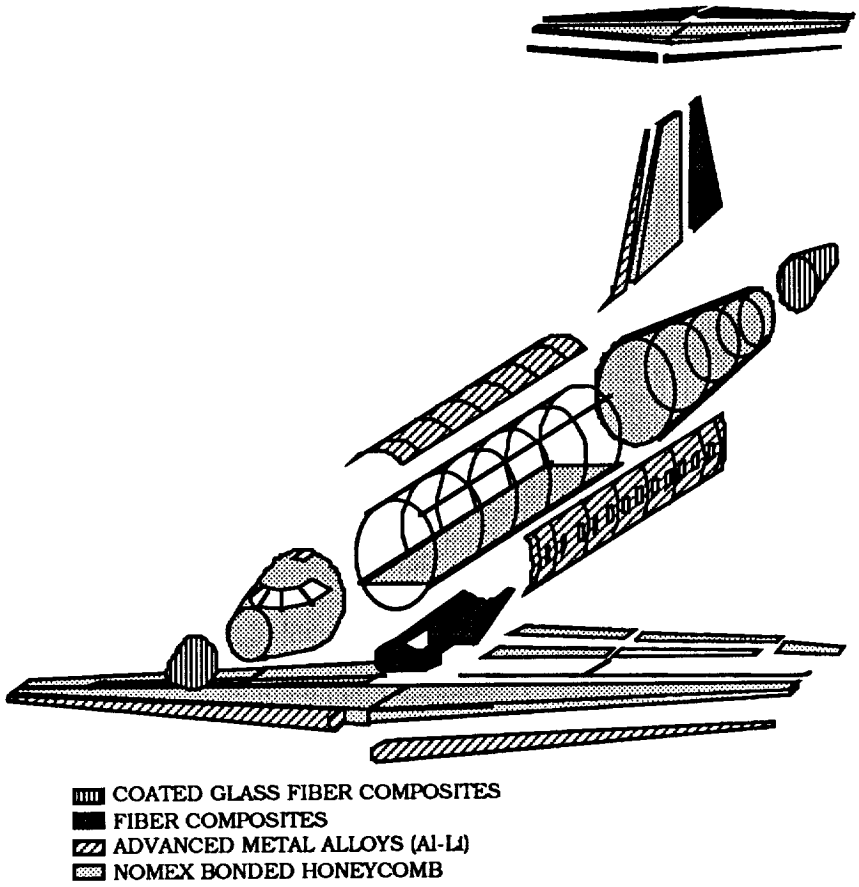

Fig. 15 Materials Distribution

Avionics

This design will use the Honeywell Primus 2000 system, which is used in the Dornier 328. This avionics system is considered to be one of the best in the world because it has tremendous capability and many functions, while having very few line-replaceable units (LRU's). The Primus 2000 system is smaller, lighter, requires less power, and is more reliable than many of the systems in existence today.[14]

Advanced technologies used in the Primus 2000 are:

1. Surface mount technology
2. Very large scale integrated circuits
3. Application-specific integrated circuits
4. High-density, multi-layer circuit boards.

Major components and subsystems are:

1. Integrated avionics computer
2. Electronic displays
3. Attitude and heading reference system
4. Micro air data computer
5. Weather radar
6. Primus-II radio package
7. Options including: Global positioning system
   Inertial reference system
   Traffic alert and collision avoidance system.

Cost Analysis

The cost of an aircraft in the design phase is extremely difficult to analyze. Cost projection to any degree of accuracy is virtually impossible due to the unpredictability of the economy from year to year. Therefore, it is difficult to base current design costs on the costs of existing aircraft. To evaluate the cost of a single airplane is relatively meaningless because total unit cost decreases with respect to production quantity. As a result, we

conducted a full-scale component cost estimation based on variable production quantities.

The three main components costs investigated were manufacturing materials, avionics, and engine costs. The following formulas were used to generate a stacked-bar graph to illustrate the various cost ranges:

$$\text{Mfg. Cost} = \frac{11.0\, W_e^{.921} V^{.621} Q^{.799}}{Q},$$

$$\text{Engine cost} = \frac{2{,}000{,}000\, Q^{.955}}{Q},$$

$$\text{Avionics cost} = 20\% \times (\text{Mfg. cost})'$$

$$\text{Materials cost} = (\text{Mfg. cost}) - (\text{Avionics cost})'$$

$$\text{Total unit cost} = (\text{Material}) + (\text{Avionics}) + (\text{Engine})' \qquad (7)$$

where W_e is empty weight, V is velocity in feet per second, and Q is production quantity per year. The cost for two engines has been quoted by Allison Gas Turbines to be $2 million. As in shown in Figure 16, total unit costs range from $6.37 million to $5.27 million on a production scale of 30 to 100 units produced per year. [2]

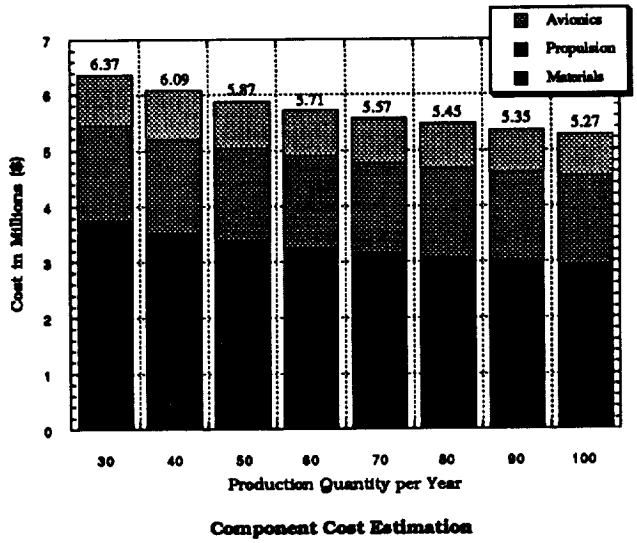

Fig. 16 Component Costs per Annual Production Quantity

Discussion

Upon completion of this report, we have found that there are still areas where more information would be beneficial. FAA and FAR regulations often set the limits for aircraft in design. This is one area where more information should be gathered and comparisons made with the performance of our aircraft. A more difficult yet useful area that needs attention is in structural analysis. This analysis, with the aid of NASTRAN, could prove to be very useful in determining structural weak or strong points. Two areas that may coincide and offer a more in depth look at the response of the aircraft are control surface response and stability. More specifically with stability, a greater concentration on how pitching moment will change with elevator deflection should be investigated.

LIST OF REFERENCES

1. Roskam, J., *Airplane Design: Part I : Preliminary Sizing of Airplanes*, Roskam Aviation and Engineering Corporation, Ottawa, KS, 1985.

2. Raymer, D.P., *Aircraft Design: A Conceptual Approach*, AIAA Lecture Series, American Institute of Aeronautics and Astronautics, Inc., Washington, D.C., 1989.

3. Shevell, R.S., *Fundamentals of Flight*, 2nd. ed., Prentice Hall, Englewood Cliffs, NJ, 1989.

4. Roskam, J., *Methods for Estimating Drag Polars for Subsonic Aircraft*, J. Roskam, Lawrence, KS, 1971.

5. *Generalized Method of Propeller Performance Estimation,* Hamilton Standard, Division of United Aircraft Corporation, Aug., 1965.

6. Federal Aviation Agency, *Federal Aviation Regulations* , Part 25, February 1, 1965.

7. Kandebo, S.W., *Aviation Week and Space Technology*, McGraw-Hill Publication, Feb. 19, 1990.

8. Riffel, R.E., et al, *The GMA 2100 and GMA 3007 Engines for Regional Aircraft*, AIAA-90-2523, 26th Joint Propulsion Conference, July 16-18, 1990.

9. Niu, M.C.Y., *Airframe Structural Design*, Conmilit Press, Ltd., New York, 1989.

10. Little, D., "Overview," Technical Paper from Airbus Industrie, Blagnac, France, provided by Dr. R.S. Gross.

11. Garrison, P., "Testing Composites' Mettle," *Flying,* Nov., 1989.

12. Kolcum, E.H., "Lockheed Expands Composite Capabilities to Meet Future Needs," *Aviation Week and Space Technology*, Sept. 8, 1986.

13. Fedrow, E., "Equipment Suppliers to the Dornier 328 Program," *Dornier Post*, Dornier, GmbH, Friedrichshafen, Germany, Feb., 1989.

14. Keller, H., Sahm, K.F., and Shroder, H.W., "Technology of Structures Maintains High Standards," *Dornier Post*, Dornier, GmbH, Friedrichshafen, Germany, Feb., 1990.